Theoretical investigations, Molecular Docking, ADMET analysis, Molecular Dynamic Simulation, and Drug-Likeness Scoring of (E)-1-[2-(3,4-Dimethylphenyl) Diazen-2-Ium-1-Yl] Naphthale...

Article *in* Turkish Computational and Theoretical Chemistry · February 2025

DOI: 10.33435/tcandtc.1530717

CITATION
1

READS
179

10 authors, including:

Youcef Megrouss
faculté des sciences exactes et informatique université de chlef algerie
37 PUBLICATIONS **429** CITATIONS
SEE PROFILE

Souheyla Chetioui
University of M'sil
54 PUBLICATIONS **130** CITATIONS
SEE PROFILE

Farah Chafika Kaouche
Université IBN Khaldoun Tiaret
9 PUBLICATIONS **9** CITATIONS
SEE PROFILE

Salem Yahiaoui
Université de Mostaganem
21 PUBLICATIONS **131** CITATIONS
SEE PROFILE

Turkish Computational and Theoretical Chemistry

Turkish Comp Theo Chem (TC&TC)

Volume(Issue): 9(3) – Year: 2025 – Pages: 57-78

e-ISSN: 2602-3237

https://doi.org/10.33435/tcandtc.1530717

Received: 10.08.2024 ***Accepted***: 21.10.2024 *Research Article*

Theoretical investigations, Molecular Docking, ADMET analysis, Molecular Dynamic Simulation, and Drug-Likeness Scoring of (E)-1-[2-(3,4-Dimethylphenyl) Diazen-2-Ium-1-Yl] Naphthalen-2-Olate as a Corticosteroid Side-Chain-Isomerase Inhibitor

Youcef Megrouss[a,b,1], Souheyla Chetioui[c,d], Chafika Farah Kaouche[e], Salem Yahiaoui[a,f], Khaled Drim[g] , Zohra Douaa Benyahlou[a], Mansour Azayez[b], Sid Ahmed Kaas[a,h], Mokhtaria Drissi[e], Abdelkader Chouaih[a]

[a]Laboratory of Technology and Solid Properties (LTPS), Faculty of Sciences and Technology, Abdelhamid Ibn Badis University of Mostaganem, MOSTAGANEM 27000, Algeria.
[b]Chemistry Department, Faculty of Exact Sciences and Informatic, Hassiba Benbouali University, Chlef 02000, CHLEF, Algeria.
[c]Faculty of Technology. University of M'sila. PO Box 166 Ichebilia, 28000 M'SILA, Algeria.
[d]Research Unit for Chemistry of the Environment and Molecular Structural. University of Constantine 1, CONSTANTINE 25000, Algeria.
[e]Laboratory of synthesis and catalyze , University Ibn khaldoun of tiaret, 14000 TIARET Algeria
[f]High Training College of Teachers-MOSTAGANEM 27000, Algeria
[g]Laboratory of Vegetal Chemistry, Water-Energy, Hassiba Benbouali University of Chlef ,02000, CHLEF, Algeria
[h]Department of material science, Faculty of science and technology, Tissemsilt university, TISSEMSILT Algeria

Abstract: In this article, the optimized structure and their associated properties of the (E)-1-[2-(3,4-Dimethylphenyl)diazen-2-ium-1-yl]naphthalen-2-olate compound (EDNO) were obtained and evaluated using The density functional theory DFT at the (B3LYP/6-311G++(d,p)) level in the gas phase, To quantify the intermolecular interactions, Hirshfeld surface(HS) analysis was used, HS and 2D fingerprints indicate H···H (52%) and C− H···C (26.7%) as the most relevant intermolecular interactions in the crystal packing of EDNO. the reduced density gradient (RDG) method was used to reveal and distinguish between attractive interactions such hydrogen bonds, repulsive interactions and van der Waals interactions. Further, molecular docking, binding free energy calculations, and ADMET prole of the title compound was carried out to determine the binding affinity and toxicity. A 100 ns molecular dynamics (MD) simulation was performed to evaluate the binding stability of the compound EDNO/2WV2 complex using Desmond. Binding free energy of the complex was computed for 100 trajectory frames using the MM-GBSA approach.

Keywords: Azo Compounds; Hirshfeld surface analysis; DFT calculations; ADMET; Molecular docking; MD simulation.

1. Introduction

The chemical (E)-1-[2-(3,4-Dimethylphenyl) diazen-2-ium-1-yl].-naphthalen-2-olate belongs to the family of azo compounds, which are distinguished by the presence of an azo group (-N=N-) that connects two aromatic structures. Azo compounds are essential in a variety of disciplines, particularly as dyes, pigments, and coloring agents in the textile and food industries [1,2]. Their chemical structure confers distinctive spectrum features, making them useful as fluorescence probes and pH indicators. Furthermore, because of

[1]Corresponding Authors
e-mail: youcefmegrouss@gmail.com/y.megrouss@univ-chlef.dz

their propensity to undergo reversible photochemical changes, these compounds have sparked interest in their possible use in optoelectronic materials and information storage devices. The growing interest in these compounds arises from their adaptability and the ability to adjust their properties via substitutions on the aromatic rings, paving the path for novel applications in chemistry and biology [3-8].

For instance, in medicinal chemistry, azo compounds have been studied for their antimicrobial and anticancer properties, demonstrating their potential as therapeutic agents [9,10]. Furthermore, their involvement in the development of advanced materials like liquid crystals and polymers highlights their importance in material science [11-14]. Azo compounds are also significant in environmental chemistry, where they are analyzed for their behavior and degradation in both natural and engineered systems. Their persistence and transformation products can affect environmental health, making it essential to understand their fate for effective environmental protection [15-17]. In analytical chemistry, azo compounds are vital as reagents and indicators, aiding in the detection and quantification of various analyses [18-20]. The ability to customize their chemical and physical properties through strategic substitutions enhances their applicability across various scientific domains, showcasing their wide-ranging and significant impact in modern science and industry.

In this article, we conducted a comprehensive study of the molecule (E)-1-[2-(3,4-Dimethylphenyl) diazen-2-ium-1-yl]-naphthalen-2-olate. Our study began with experimental structural determination using X-ray diffraction, followed by a comparison with the theoretically determined geometry via density functional theory (DFT) using the B3LYP functional with the basis set 6-311G++(d,p). The agreement between theoretical and experimental results confirmed the reliability of the method used, enabling us to characterize the molecule's properties. We examined the compound's intermolecular interactions using reduced Density Gradient Analysis (RDG). The RDG plot provided insights into steric effects, repulsive interactions, and hydrogen bonding within the compound. Notably, steric repulsion was most apparent in the aromatic and benzene rings, while the presence of green regions indicated hydrogen bonding interactions. Complementing this analysis, we utilized a Hirshfeld (HS) surface analysis to visually illustrate the contributions of intermolecular interactions through a 2D fingerprint plot. Our findings revealed that hydrogen-hydrogen (H---H) interactions were predominant, constituting 52.0% of the total, whereas oxygen-oxygen (O---O) interactions were relatively rare, comprising just 0.2%. This detailed analysis of intermolecular interactions has enabled us to gain a better understanding of protein-ligand interactions, which are essential for biological processes. These interactions also play a crucial role in the design of new drugs based on molecular structure. To explore the structure-activity relationship and study interactions with the appropriate target protein, we carried out a molecular docking study for the compound under study. In addition, we assessed the quality and similarity of the drug. Finally, we reinforced our biological study with a molecular dynamics simulation, confirming the stability of the complex formed between our compound and the protein, thus validating the application of our compound as a potential active ingredient in a drug.

2. Computational Method

For the theoretical calculation part ,DFT calculations were carried out using the Gaussian 16 software [21] and the Gauss View 6 program [22] . The hybrid functional B3LYP with the basis set 6-311G++(d,p) was used in all calculations. The experimental X-ray structure was used as starting geometry for the optimization task. The Hirshfeld surface maps and fingerprint plots were performed using Crystal Explorer 21.5 program [23]. Using the Multiwfn software [24], the scatterplots of the reduced density gradient (RDG) were carried out. Similarly, the 3D isosurfaces are visualized with the use of VMD software [25]. The study of ligand-protein interactions is performed using AutoDock Vina [26] AutoDock Tools [27] and Discovery Studio Visualizer [28] to prepare the target and the ligand, perform molecular docking and visualize the result respectively. The Molecular Dynamics (MD) simulation was conducted using the Desmond Package from the Schrödinger software suite.

3. Results and discussion

3.1. Molecular geometry

The comparison between experimental (X-ray) and computational (B3LYP/6-311G++(d,p)) results reveals several noteworthy observations regarding the structural properties of the (E)-1-[2-(3,4-Dimethylphenyl)diazen-2-ium-1-yl]-naphthalen-2-olate compound, The molecular structure with atomic labeling is depicted in Fig.1.

Generally, the computed bond lengths closely match the experimental values, indicating the accuracy of the computational approach in predicting molecular geometry. The C–C distances in both benzene rings, as measured experimentally and calculated, are nearly identical, hovering around 1.38 Å, which aligns well with established values in the literature [29]. The N-N distance is 1.2946 Å (X-ray) and 1.30231 Å (B3LYP). The O-C distance is 1.2873 (X-ray) and 1.25266Å (B3LYP). The bond angles derived from computational methods align well with experimental measurements, such as the bond angle of N2—N1—C9 is 117.66° (X-ray) and 120.00° (B3LYP), suggesting consistency in the molecular conformation predicted by theory and observed experimentally.

Dihedral angles, crucial for understanding molecular conformations, exhibit good agreement between experimental and computational data, the dihedral angle of C9—N1—N2—C11A is −178.13◦ (X-ray) and -179.99° (B3LYP), indicating reliable predictions of molecular orientation.

The congruence between experimental and computational results underscores the efficacy of the computational approach (B3LYP/6-311G++(d,p)) in elucidating the structural characteristics of the title compound molecule. These findings provide valuable insights for further investigations into the chemical and physical properties of the title compound and its potential applications.

Table 1. Geometric parameters (Å)

Bond lengths (Å)	**X-ray**	**B3LYP/6-311G++(d,p)**
O1—C8	1.2873 (15)	1.25266
N1—N2	1.2946 (15)	1.30231
N1—C9	1.3555 (15)	1.32768
N2—C11A	1.385 (3)	1.40301
C1—C2	1.373 (2)	1.38566
C2—C3	1.400 (3)	1.40199
C3—C4	1.366 (2)	1.38355
C4—C5	1.404 (2)	1.40774
C5—C6	1.4316 (19)	1.44258
C6—C7	1.3465 (19)	1.35389
C7—C8	1.4390 (17)	1.45127
C8—C9	1.4335 (17)	1.47258
C11A—C12A	1.394 (3)	1.39651
C11A—C16A	1.382 (4)	1.3985
C12A—C13A	1.380 (3)	1.38987
C13A—C14A	1.379 (4)	1.39703
C14A—C17A	1.510 (3)	1.50816
C14A—C15A	1.398 (4)	1.41249
C15A—C18A	1.497 (4)	1.50934
C15A—C16A	1.401 (4)	1.39302
Bond angles (◦)	**X-ray**	**B3LYP/6-311G++(d,p)**
N2—N1—C9	117.66 (10)	120.003
N1—N2—C11A	123.10 (13)	121.94333
C1—C2—C3	120.47 (15)	120.64249
C2—C3—C4	119.93 (15)	119.39191
C3—C4—C5	120.95 (13)	120.87337
C4—C5—C6	121.55 (12)	120.868
C5—C6—C7	122.30 (12)	122.73247
C6—C7—C8	121.03 (12)	121.50359
O1—C8—C7	119.95 (11)	121.19842
O1—C8—C9	121.64 (11)	121.60896

C7—C8—C9	118.41 (11)	117.19263
N1—C9—C8	123.86 (11)	122.95671
N2—C11A—C12A	119.43 (19)	117.8906
N2—C11A—C16A	120.6 (2)	122.34552
C12A—C11A—C16A	120.0 (2)	119.76388
C11A—C12A—C13A	119.3 (2)	119.28076
C12A—C13A—C14A	121.8 (2)	121.84916
C13A—C14A—C15A	119.0 (2)	118.54908
C15A—C14A—C17A	121.0 (2)	121.09417
C13A—C14A—C17A	120.0 (2)	120.35675
C14A—C15A—C16A	119.6 (2)	119.70719
C14A—C15A—C18A	120.7 (2)	120.64581
C16A—C15A—C18A	119.7 (3)	119.647
C11A—C16A—C15A	120.3 (3)	120.84992
Dihedral angles (◦)	**X-ray**	**B3LYP/6-311G++(d,p)**
C9—N1—N2—C11A	−178.13 (15)	-179.99694
N2—N1—C9—C8	2.05 (17)	-179.99449
N1—N2—C11A—C12A	177.29 (17)	-180.00
N1—N2—C11A—C16A	−4.1 (3)	0.00
C1—C2—C3—C4	−0.1 (3)	0.00
C2—C3—C4—C5	−0.1 (2)	0.00
C3—C4—C5—C6	179.81 (14)	-180.00
C4—C5—C6—C7	−179.60 (13)	-180.00
C5—C6—C7—C8	0.1 (2)	0 .00
C6—C7—C8—O1	−179.29 (12)	179.99802
C6—C7—C8—C9	1.69 (19)	-0.0007
O1—C8—C9—N1	−4.99 (19)	0.00234
C7—C8—C9—N1	174.01 (11)	-179.99894
N2—C11A—C12A—C13A	179.48 (19)	180.00
C16A—C11A—C12A—C13A	0.8 (4)	0.00
N2—C11A—C16A—C15A	−179.0 (2)	-180.00
C12A—C11A—C16A—C15A	−0.4 (4)	0.00029
C11A—C12A—C13A—C14A	−0.4 (3)	0.00
C12A—C13A—C14A—C15A	−0.6 (3)	0.0003
C12A—C13A—C14A—C17A	−179.8 (2)	-179.99886
C13A—C14A—C15A—C16A	1.1 (4)	0.00
C13A—C14A—C15A—C18A	−177.2 (2)	-179.9978
C17A—C14A—C15A—C16A	−179.7 (2)	179.99895
C17A—C14A—C15A—C18A	2.0 (3)	0.00136
C14A—C15A—C16A—C11A	−0.6 (4)	0.00
C18A—C15A—C16A—C11A	177.7 (2)	179.99753

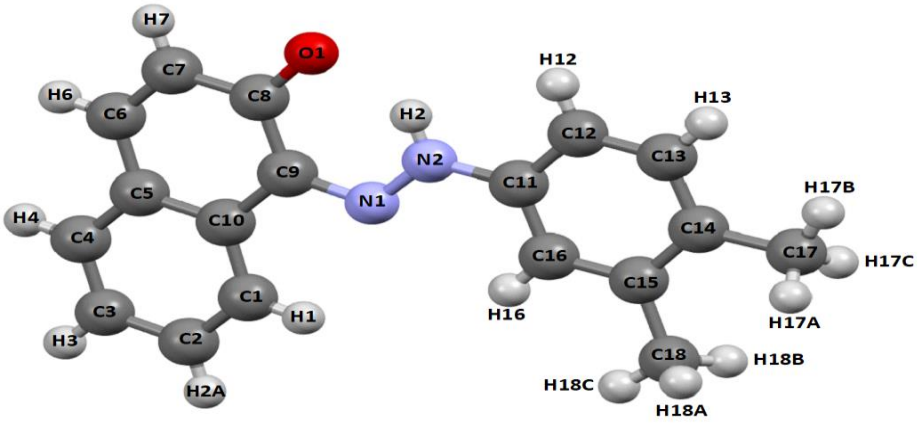

Figure 1. 3D structure of EDNO with atomic labeling.

3.2. RDG (Reduced Density Gradient Analysis)

We conducted the topological analysis to delve into the subtle interactions between various compounds in greater detail. The Atoms in Molecules (AIM) theory is widely employed for this purpose, as it allows us to identify different types of interactions across various molecular systems and analyze the electron density at critical binding points (BCP) [30]. By utilizing topological parameters such as bond energy (E int = V(r)/2), kinetic Hamiltonian energy (H(r) = G(r) + V(r)), potential energy density (V(r)), Lagrangian kinetic energy (G(r)), electron density Laplacian (∇2 ρ(r)), and electron density (ρ(r)), we were able to observe hydrogen bonding properties among the compound structures. We used an optimized geometric structure to pinpoint critical bond points (BCP) and ring critical points (RCP) within the CEFP crystal structure. The analysis was conducted using the Multiwfn program [24]. Figure 2 displays scatter diagrams and gradient isosurfaces representing the title compound. In Figure 2, we observe the molecular interactions' patterns within the RCP and BCP, as identified by the Multiwfn software. At a ρBCP value of 0.01 and a Laplacian value of 0.03, electron density indicates molecular stability. Molecular stability hinges on various interactions, including both intra- and intermolecular forces. These interactions can be discerned through reduced density gradient (RDG) analysis, a method rooted in the examination of non-covalent interactions (NCI) within the system [31]. In Figure 2 (a), we present the NCI-RDG analysis conducted with an isosurface value of 0.5. The reduced density gradient (RDG) encompasses fundamental aspects, involving density and its first derivative, as outlined in prior literature [32]. The RDG isosurface surrounding specific regions delineates the interactions among molecules, as illustrated in Figure 2 (b). The dotted red areas signify steric effects, indicating repulsive interactions. Notably, the most pronounced steric repulsion occurs at the centers of two aromatic rings engaged in π-π stacking interactions [33], as well as at the benzene ring, highlighted in the RDG chart as the red zone. The overlapping red and green regions around the (O, H) of the two benzene rings and (C, C) of the methyl group denote repulsive areas. Conversely, the green regions denote hydrogen-bonding interactions, which contribute to the stability of the title compound's molecular system.

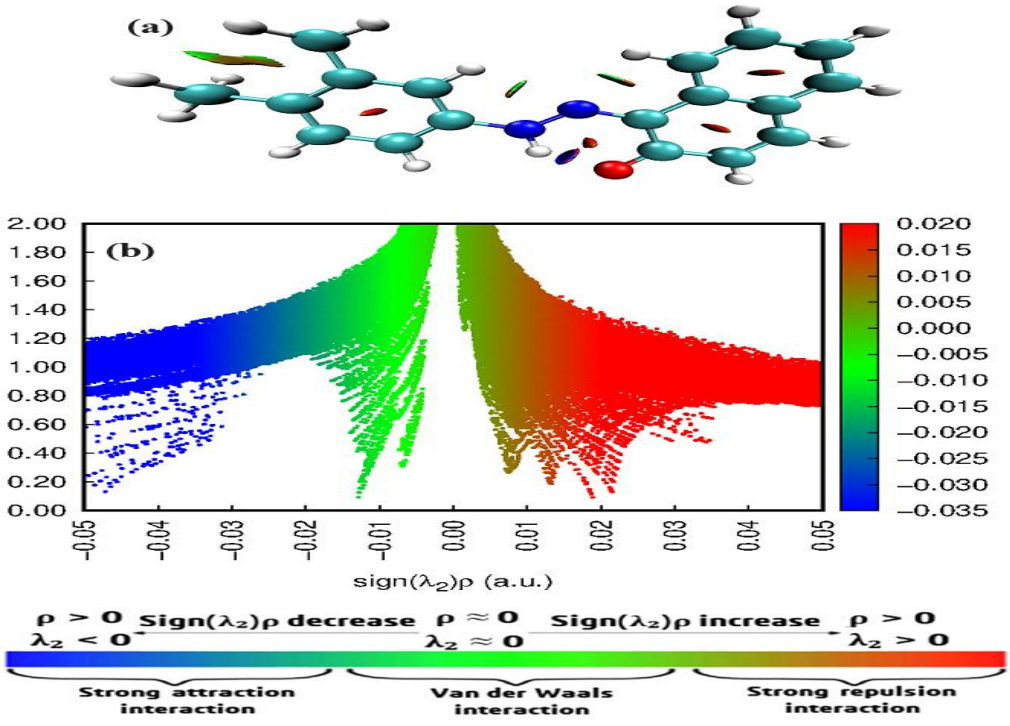

Figure 2. (a) the gradient isosurfaces and (b) the scatter diagram of the title compound

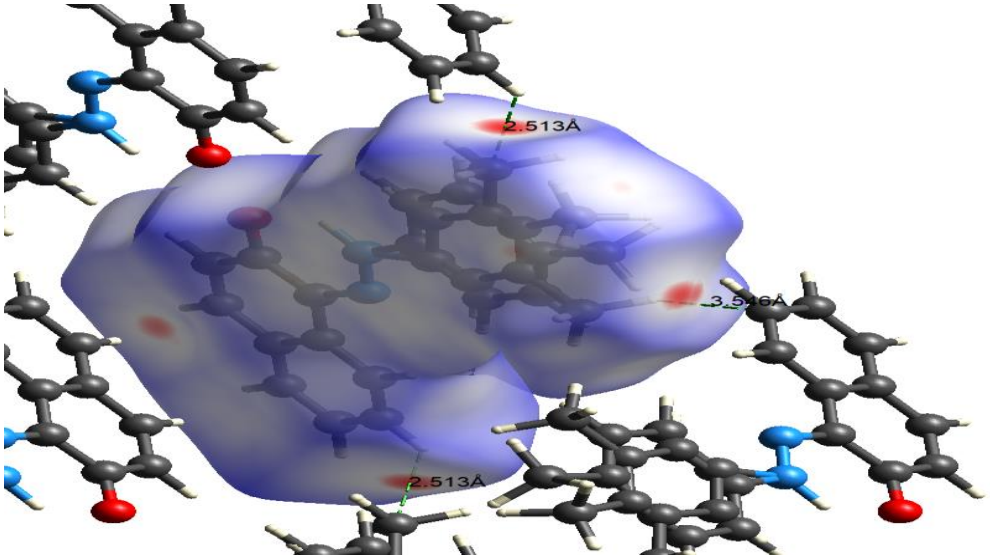

Figure 3. Intermolecular interactions represented in red circle point collapsing on the *d* norm area in b-axis for the crystal structure of the title compound.

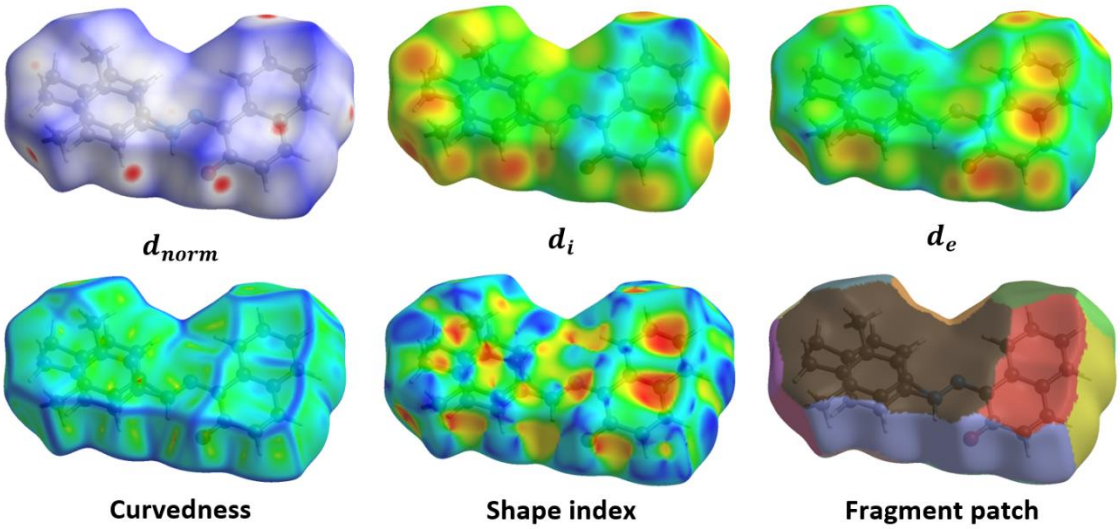

Figure 4. Hirshfeld surface analysis of the title compound with d e, d i, d norm, shape index, curvedness, and fragment patch

3.3. Hirshfeld Surface (HS) analysis

Hirshfeld Surface (HS) analysis is a technique that divides molecular crystal space into discrete, non-overlapping molecular entities. With the development of HS fingerprint plots [34], which provide an easily understood representation of intermolecular contacts in crystals, significant advancements occurred. Further developments include the use of decoration, a mapping method that applies a color scale onto the HS to graphically represent scalar properties and quickly obtain insights into molecular environments in the crystalline state [35]. Feature decomposition is another innovation that helps identify specific interactions. The Crystal Explorer 21.5 [36] package was utilized to examine Hirshfeld surfaces and their corresponding fingerprint plots. The crystallographic information file (CIF) was used to enter the required data for this analysis [37]. Fig. 3 shows the three-dimensional Hirshfeld surface plot on d_{norm}. The visualization illustrates the interactions between hydrogen and carbon atoms by revealing four different red dots, the distance between nearby molecules is 2.513 Å. Fig. 3, illustrates the Hirshfeld surface analysis (HSA) conducted on the title molecule, presenting results via parameters such as d norm, d e, d i, shape index, fragment patch, and curvedness. Notably, the shape

index map reveals the presence of π-π stacking interactions among molecules, as indicated by adjacent blue and red triangles. Fig. 4 displays the fingerprint plot (100%) of the title compound, specifically plotting d_i against d_e. This plot illustrates the distances between nuclei starting from the surface and the nearest nuclei within the molecule's surface, spanning from 0.9050 to 2.5474 Å. Fig. 4, displays by illustration how the Hirshfeld surface (HS) contributes to the overall molecular surface. It also highlights the specific proportions of different types of intermolecular contacts within the molecule. Essentially, it visually breaks down the contributions of intermolecular interactions using 2D fingerprint plotting. The most prevalent interactions involve hydrogen (H···H) interactions, constituting 52.0% of the total. This dominance is attributed to the abundance of hydrogen atoms on the surface of CEFP. Following closely are carbon-hydrogen (C···H/H···C) interactions, contributing 26.7%. Additionally, carbon-carbon (C···C) interactions make up 5.8% of the total. Furthermore, nitrogen-hydrogen/hydrogen-nitrogen (N···H/H···N) interactions account for 4.5%, while oxygen-carbon/carbon-oxygen (O···C/C···O) interactions represent 0.3%. A minimal contribution is seen from oxygen-oxygen (O···O) interactions, constituting only 0.2%. These proportions are visualized in Figure 5.

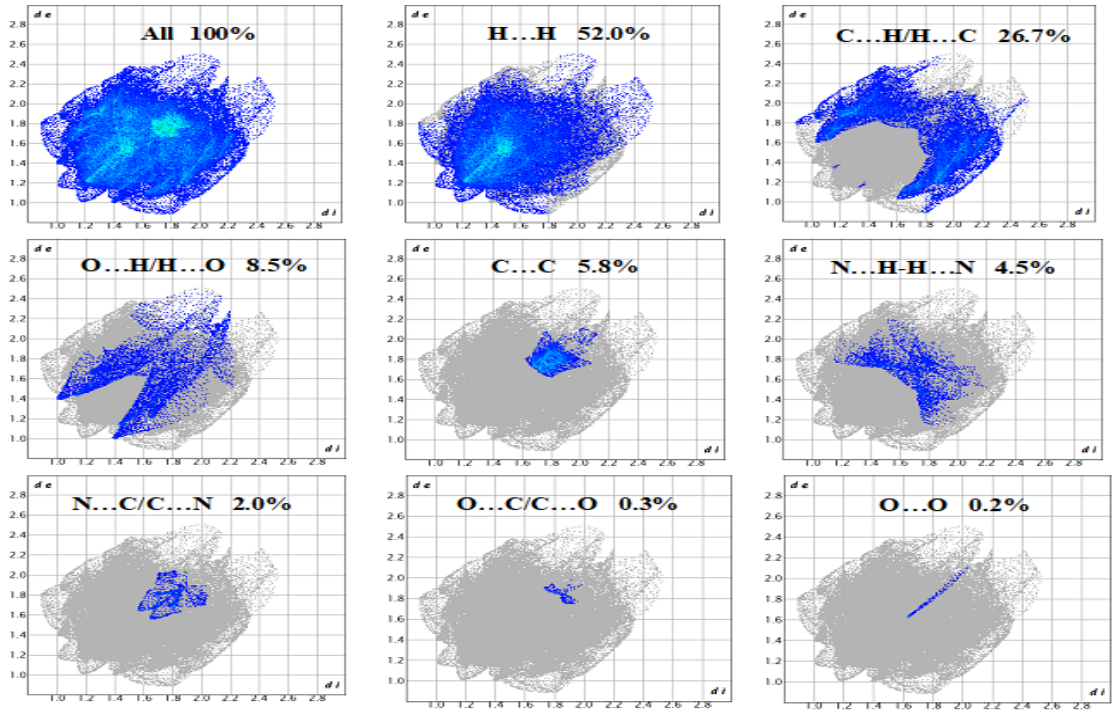

Figure 5. 2D fingerprint graphs depicting the total contributions to the total HS surface region and the single percentages of the different intermolecular interactions.

3.4. Prediction of Activity Spectra for Substances (PASS) analyses

PASS (Prediction of Activity Spectra for Substances) is a crucial computational tool in cheminformatics and drug discovery. It predicts the biological activities of chemical compounds by analyzing their structural formulas and drawing from a knowledge base of structure-activity relationships (SAR) derived from experimental data [38]. This tool is invaluable in early drug development stages, assisting researchers in narrowing down the pool of compounds for further investigation. Available at http://way2drug.com/PassOnline, the PASS Software can predict over 4000 types of biological activity, including pharmacological effects, mechanisms of action, toxic and adverse effects, and interactions with metabolic enzymes and transporters [39]. It claims an impressive 90% validity rate. The outcomes of PASS calculations are expressed as Pa (probability of active molecule) and (probability of inactive molecule) [40]. A Pa value of 0.7 or higher indicates a high likelihood of experimental pharmacological activity, while

values between 0.5 and 0.7 suggest a lower likelihood. A Pa value below 0.5 indicates a lower likelihood of discovering activity through experimentation but may also imply a chance of discovering a novel chemical [41]. These parameters guide researchers in prioritizing compounds for further experimental investigation. The results presented in Table 2 were interpreted and applied flexibly. (EDNO) compound exhibited the highest Pa value (0.731) and a Pi value of 0.007 for its activity as a corticosteroid side-chain isomerase inhibitor. This type of medication functions by inhibiting the enzyme corticosteroid side-chain isomerase [42]. This enzyme plays a crucial role in the synthesis of corticosteroids, hormones that are involved in various physiological processes, including immune response, metabolism, and stress regulation [43, 44]. One example of a corticosteroid side-chain isomerase inhibitor is aminoglutethimide, which was historically used to treat Cushing's syndrome [45]. Another example of a corticosteroid side-chain isomerase inhibitor is fluconazole. Although primarily used as an antifungal medication, fluconazole can also inhibit the enzyme 14-alpha-demethylase, which plays a role in cortisol synthesis [46].

Table 2. PASS prediction results of the title compound.

Pa	Pi	Activity
0,731	**0,007**	**Corticosteroid side-chain-isomerase inhibitor**
0,642	**0,007**	**Histamine release inhibitor**
0,643	**0,014**	**Platelet aggregation stimulant**
0,691	**0,072**	**Ubiquinol-cytochrome-c reductase inhibitor**
0,631	**0,015**	**Aspartate-phenylpyruvate transaminase inhibitor**
0,636	**0,025**	**2-Dehydropantoate 2-reductase inhibitor**
0,636	**0,032**	**Glucose oxidase inhibitor**
0,612	**0,014**	**Amine dehydrogenase inhibitor**
0,621	**0,026**	**Alkane 1-monooxygenase inhibitor**
0,665	**0,075**	**Aspulvinone dimethylallyltransferase inhibitor**

Table 3. Physicochemical and Pharmacokinetic properties of the title molecule.

Parameters	Values
Molecular weight	**276.33g/mol**
FLEX Number of rotatable bonds	**2**
Num. heavy atoms	**21**
Number of H-bond acceptors	**2**
Number of H-bond donors	**1**
Molar Refractivity	**86.84**
TPSA (Polarity)	**41.46Å²**
Log $P_{o/w}$ (iLOGP) (Lipophilicity)	**2.46**
Consensus Log $P_{o/w}$ (Lipophilicity)	**4.37**
POLAR (Polarity)	**Moderately soluble**
GI absorption	**High**
Blood Brain Barrier (BBB) Permeability	**Yes**
CYP1A2 inhibitor	
CYP2C19 inhibitor	**Yes**
CYP2C9 inhibitor	**Yes**
CYP2D6 inhibitor	**Yes**
CYP3A4 inhibitor	**No**
Log K_p (skin permeation)	**No**
Lipinski	**-4.88cm/s**
Ghose, Veber, Egan, and Muegge	**Yes; 0 violation**
Bioavailability Score	**Yes**
Synthetic accessibility	**0.55**
	3.26

3.5. Druglikeness and ADMET analysis

Pharmaceutical companies invest heavily in drug discovery, but clinical trial failures due to pharmacokinetic issues or toxicities are costly. AI-based computational methods, such as machine learning, leverage data to predict these properties, including absorption, distribution, metabolism, excretion, and toxicity (ADMET), potentially reducing risks and accelerating drug development [47]. ADMET profiling is a critical step in drug development, involving the assessment of a compound's Absorption, Distribution, Metabolism, Excretion, and Toxicity. These properties determine a drug's efficacy and safety [48]. The SWISS ADME tool is a widely used web-based application that evaluates the physicochemical properties of drug candidates. This tool provides reliable predictive testing for several key parameters: Absorption evaluates how well a compound is absorbed into the bloodstream. Distribution predicts the distribution of the compound throughout the body and its potential to reach target tissues. Metabolism assesses the compound's metabolic stability and the likelihood of it being broken down by the body. Excretion predicts the routes and rates at which the compound is excreted from the body. Toxicity assesses the potential toxic effects of the compound [49]. Using the SWISS ADME tool involves inputting the molecular structure of a compound to receive predictions on its ADMET properties. In silico ADMET analysis utilizes computational models, such as Lipinski's Rule of Five, which considers factors like molecular weight, the number of hydrogen bond acceptors and donors, and the logP value. Compounds that do not meet these criteria are likely to have poor bioavailability [50]. Recent advancements in machine learning have improved the accuracy of ADMET predictions by analyzing large datasets, significantly reducing the time and costs in drug development [51]. The drug-likeness parameters of the little compound are a reported in Table 3 and were expressed by the Lipinski's rule of five. According to this guideline, oral medications must meet the following requirements: POLAR (Polarity): 20Å 2 < TPSA < 130Å2, LIPO [Lipophility]: -0.7 < XLOGP3 < +5.0, INSOLU [Insolubility]: -6 < Log S (ESOL) < 0, FLEX [Flexibility]: 0< Num. rotatable bonds < 9, size: 150g.mol-1< MV < 500g.mol-1, INSATU [Insaturation]: 0.25 < Fraction Csp3 < 1 [52]. The results indicate that the title compound aligns well with Lipinski's Rule of Five, suggesting favorable bioavailability. Additionally, rule-based filters from Lipinski, Ghose, Veber, and Egan were employed to evaluate the predicted drug-like properties of the compound. The compound has two rotatable bonds, which is a crucial parameter for molecular flexibility and should be less than 10. The TPSA is within the acceptable range, indicating that the compound has suitable physicochemical properties to be used as a pharmaceutical drug candidate. The BOILED-Egg model classifies molecules based on their likelihood of intestinal absorption (HIA) and blood-brain barrier (BBB) penetration. The compound is predicted to have good permeability through the blood-brain barrier, excellent intestinal absorption, and it is not a substrate for P-glycoprotein, suggesting favorable pharmacokinetic properties for oral administration and central nervous system targeting. This comprehensive analysis indicates that the compound meets all the criteria for drug-likeness according to Lipinski's Rule of Five and is well-suited for further drug development and testing.

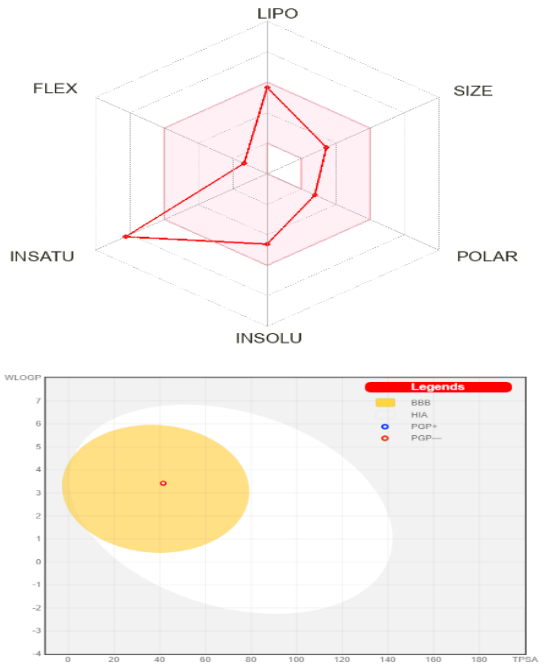

Figure 6. a) Oral bioavailability radar and b) blood-brain barrier (BBB) permeability [BOILED-Egg] diagram of title compound.

3.6. Molecular docking against targeted receptor

In recent years, Molecular Docking has become integral to in-silico drug development. This method predicts how small molecules interact with proteins at the atomic level, aiding in understanding biochemical processes [53]. It relies on high-resolution 3D representations of target proteins obtained through techniques like X-ray crystallography. Molecular Docking facilitates the study of small molecule behavior within protein binding sites, including nutraceuticals. Its structure-based approach is essential for accurate predictions. [54] According to the results of PASS prediction, the target protein is identified with PDB ID: 2WV2 (Method: X-ray diffraction, Resolution: 2.70 Å) was downloaded from protein database website (https://www.rcsb.org) [55]. The PDB ID: 2WV2 represents the crystal structure of the enzyme responsible for cholesterol biosynthesis, human lanosterol 14-alpha demethylase (CYP51). [56]. The CYP51 gene is highly conserved throughout different species, and it performs a comparable function in the manufacture of sterols in both fungi and humans [57]. The structural similarities between CYP51 in humans and fungi makes it a crucial target for antifungal medications, as inhibitors can impact both types of enzymes [58]. Comprehending the mechanism of action of 2WV2 aids in the development of specific antifungal drugs that specifically target fungal CYP51 while minimizing any adverse effects on the human enzyme.

3.7. Protein preparation

The protein preparation was conducted using BIOVIA Discovery Studio Visualizer [28]. This procedure involved selecting the target protein, removing water molecules, heteroatoms, and co-ligands from the active site, and then adding polar hydrogen atoms [59]. The final protein structure was saved in the .pdb format. The molecular docking of the little compounds was performed using AutoDock vina program [26].

3.8. Docking and interactions study

Docking simulations were conducted, which involved creating a 3D grid box with the following dimensions: center x=-48.422, center y=11.915, center z=1.617, and grid cells of 28x28x28 $Å^3$. The selection of this grid design was purposely made to thoroughly cover the active site pocket of the target molecules. AutoDock is used to assess the binding affinity of the ligand, which helps in identifying the most favorable ligand structure and rotation in relation to the receptor (protein). Table 4 provides the binding energies and RMSD values for the nine potential conformations of the synthesized ligand in (PDB ID: 2WV2) .Based on the findings, it can be concluded that the optimal docking position is in mode 1, with a binding energy of -10.2 kcal/mol. The binding energy suggests a docking position that is highly favorable, similar to the highest scores shown in molecular docking studies for strong interactions between a ligand and receptor [57]. Mode 1 has both the highest binding affinity and an RMSD value of 0.000, indicating a flawless match with no deviation. This highlights its stability and optimal interaction inside the binding pocket. The compound was found to interact with various amino acid residues via hydrogen bonding and hydrophobic interactions. It was further revealed that the hydrophobic interactions with various amino acid residues of CYP51 occur through the three aromatic rings in the compound. The detailed description of the types of interactions and the interacting amino acid residues is presented in Table 5. Two amino acid residues, namely SER296 and GLY428, interacted to form conventional hydrogen bonds with distances of 2.04184 Å and 3.22652 Å, respectively. This compound showed Pi-alkyl interactions with PRO355, LEU356, CYS422, and ALA291. The alkyl interactions of the compound occurred with ALA288, ALA291, and LEU134. Pi-Pi T-shaped interactions were formed when two aromatic rings were oriented perpendicular to each other, resembling a "T" shape, with one aromatic ring's edge facing the plane of the other aromatic ring, involving PHE415. Additionally, the compound also showed Pi-Sigma and amide-Pi stacked interactions with THR295 and ALA291, respectively. These interactions contribute to the stability, good affinity, and highest activity. Fig. 7 provides a visual representation of the intramolecular interactions. Part (a) shows the schematic diagram of the interactions including van der Waals, hydrogen bonds, and Pi interactions. Part (b) illustrates the 3D molecular docking pose within the binding pocket. Parts (c) and (d) offer additional perspectives, highlighting the spatial

arrangement and interaction details of the compound within the protein structure. The study's comprehensive approach, including both quantitative (binding affinities, RMSD values) and qualitative (interaction types and distances) data, offers a thorough analysis of the docking results. The compound shows a strong binding affinity and stability through various interactions, making it a promising candidate for further studies.

Table 4 AutoDock Vina results of the binding affinity and RMSD values of different poses in little compound inhibitor of 2WV2.

Mode	Affinity (kcal/mol)	RMSD l.b	RMSD u.b.
1	**-10.2**	**0.000**	**0.000**
2	**-10.0**	**1.622**	**7.210**
3	**-9.3**	**3.484**	**7.066**
4	**-8.8**	**2.012**	**7.013**
5	**-8.6**	**2.109**	**7.852**
6	**-8.5**	**3.714**	**5.702**
7	**-8.4**	**5.581**	**9.773**
8	**-8.4**	**5.474**	**7.419**
9	**-8.4**	**3.866**	**5.402**

Table 5. Distances. Types and location of intermolecular interactions formed from the residues of (PDB ID: 2WV2) and the molecule.

Protein	Residues	Atom/group of compound	Category	Types	Distance (Å)
PDB(ID : 2WV2)	**A:SER296**	**O1**	**Hydrogen Bond**	**Conventional Hydrogen Bond**	**2.042**
	A:GLY428	**O1**	**Hydrogen Bond**	**Carbon Hydrogen Bond**	**3.227**
	A:THR295	**naphthalen rings**	**Hydrophobic**	**Pi-Sigma**	**3.706**
	A: PHE415	**naphthalen rings**	**Hydrophobic**	**Pi-Pi T-shaped**	**4.768**
	A:PHE415	**naphthalen rings**	**Hydrophobic**	**Pi-Pi T-shaped**	**4.642**
	A:ALA291	**Dimethylphenyl ring**	**Hydrophobic**	**Amide-Pi Stacked**	**4.459**
	A: ALA288	**C17 Dimethyl phenyl ring**	**Hydrophobic**	**Alkyl**	**3.819**
	A: ALA291	**C18 Dimethyl phenyl ring**	**Hydrophobic**	**Alkyl**	**3.617**
	A: LEU134	**C17 Dimethyl phenyl ring**	**Hydrophobic**	**Alkyl**	**4.394**
	A: PRO355	**naphthalen rings**	**Hydrophobic**	**Pi-Alkyl**	**5.264**
	A: LEU356	**naphthalen rings**	**Hydrophobic**	**Pi-Alkyl**	**5.152**
	A: CYS422	**naphthalen rings**	**Hydrophobic**	**Pi-Alkyl**	**5.182**
	A: ALA291	**Dimethylphenyl ring**	**Hydrophobic**	**Pi-Alkyl**	**4.929**

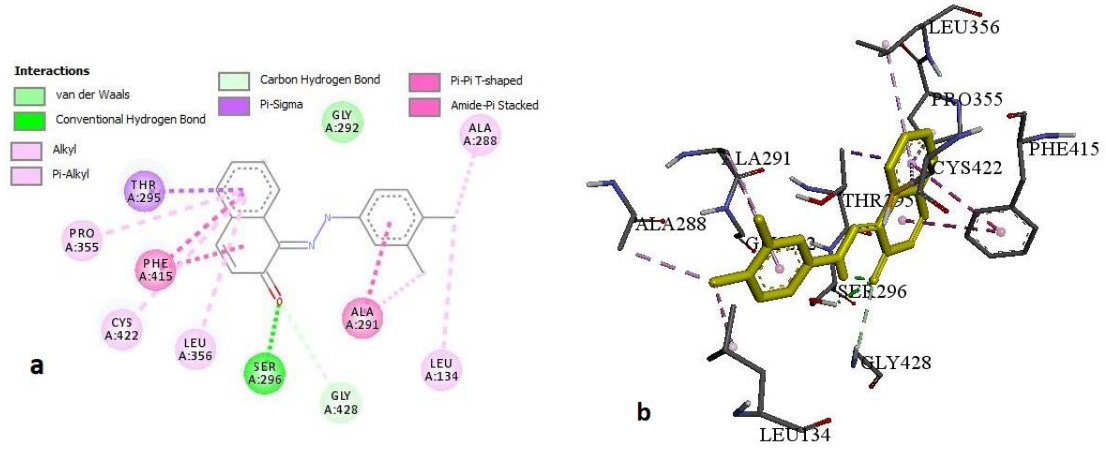

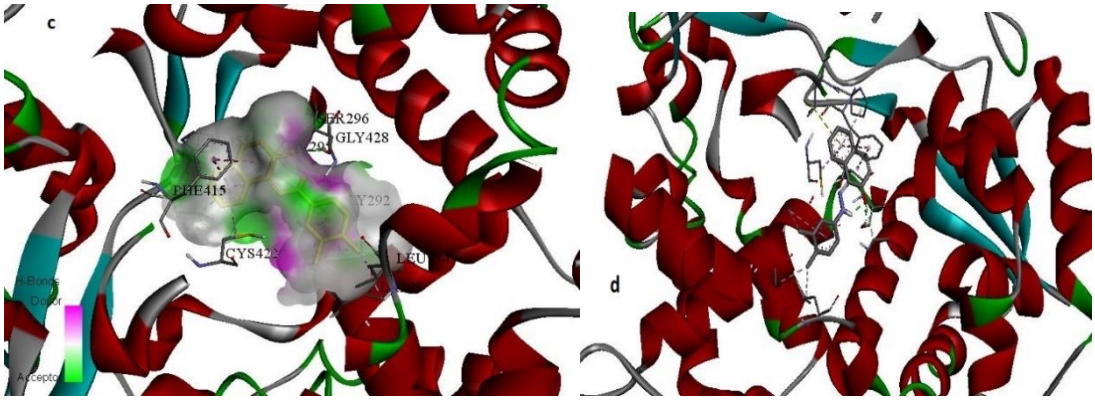

Figure 7. Intramolecular interactions that connect the structure to the 2wv2 protein

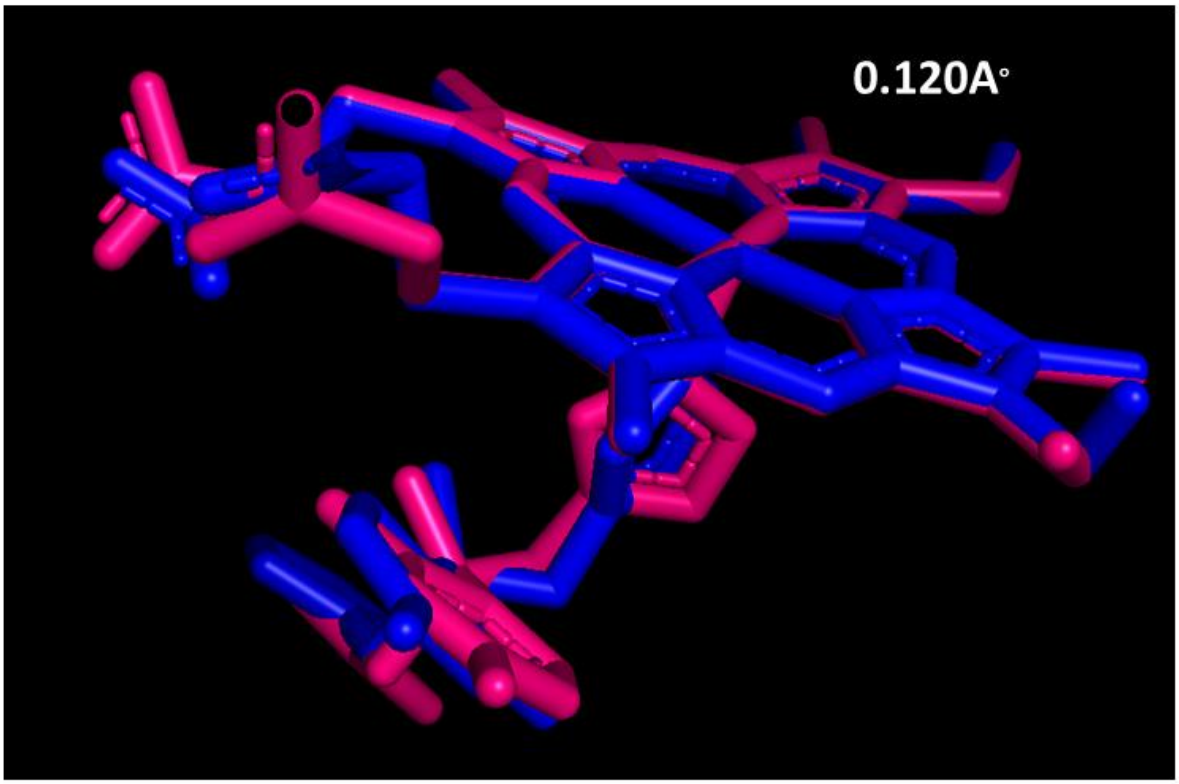

Figure 8. Validation of docking procedure through RMSD calculation of superimposed ligand Poses: retrieved and re-docked co-ligand in protein x-ray crystal structure (ID:2WV2).

3.9. Docking validation

The docking process was validated through removing the present co-ligand inside the protein active site (ID: 2WV2), re-docking it using the same protocol including the grid parameters was unchanged in the process. It was done to ensure the inhibitor binds exactly to the active site cleft and must show less deviation compared to the actual co-crystallized complex. The re-docked complex was then superimposed on to the reference co-crystallized complex using PyMOL 2.3 and the root mean square deviation (RMSD) was calculated (Fig. 8). The co-ligand bound exactly to the active site with good binding energy of −8.12 kcal/mol and RMSD of 0.12 A° (<2A°).

3.10. Methodology of molecular dynamics simulation

The Molecular Dynamics (MD) simulation was conducted using the Desmond Package from the Schrödinger software suite [60], leveraging CUDA support on Nvidia RTX 3060Ti GPU machines. For this study, the top-docking scored model of the studied compound, Mol, along with the co-ligand

Fluconazole (CID: 3365) as a reference, were selected as the starting coordinates. Before solvation, the complex was optimized, and its energy minimized using the OPLS_2005 force field, which is known for its accuracy in predicting molecular geometries, conformational energies, and non-bonded interactions for proteins and small molecules [61]. Each system was then solvated using a three-point (TIP3P) water model within cubic periodic boundary conditions measuring 100 × 100 × 100 Å, ensuring at least 10 Å of space between the protein and the edges of the simulation box. Simulations were performed under physiological conditions at pH 7.0 in an NPT ensemble (constant number of particles, pressure, and temperature) with settings of 1 atm and 303.15 K, considering the expected ionization states of protein residues and utilizing periodic boundary conditions.

3.11. Results of molecular dynamics simulations

Molecular dynamics simulations were performed for 100 nanoseconds on both the studied ligand Mol and the reference co-ligand STD, in complex with the target protein sterol 14α-demethylase, also known as CYP51 (PDB ID: 2WV2). The primary objective was to evaluate the stability of the ligand Mol in comparison to the co-ligand STD within the protein's catalytic site. To achieve this, various parameters were analyzed, including Root Mean Square Deviations (RMSD) to measure the structural stability over time, and Root Mean Square Fluctuations (RMSF) to assess the flexibility of the protein backbone. Additionally, solvent-accessible surface area (SASA) and radius of gyration (Rg) were calculated to evaluate the compactness and exposure of the protein. Principal Component Analysis (PCA) and free-energy landscape (FEL) plots were used to investigate the conformational changes and energy states of the system.

3.12. Root Mean Square Deviation studies (RMSD)

The resulting MD trajectory was analyzed to compute the root mean square deviation (RMSD) of the protein's backbone atoms in complex with both the studied ligand Mol and the co-ligand STD, as well as the RMSD of the ligands when fitted onto the protein. This analysis highlights the ligands' movement or shift from their initial binding site in the protein's active site. Fig. 9 shows the RMSD plot for the biomolecular systems Mol-2WV2 and STD-2WV2, providing insights into their dynamic behavior. The RMSD analysis of the protein backbone revealed average deviations of 3.17 Å for Mol and 2.49 Å for STD, indicating comparable stability of the protein with both the studied ligand and the co-ligand. The RMSD values for the ligands fitted onto the protein were also analyzed, with average deviations of 2.47 Å for Mol and 1.9 Å for STD within the protein's catalytic site. Both ligands demonstrated significant stability, as indicated by their lower deviations (Fig. 9).

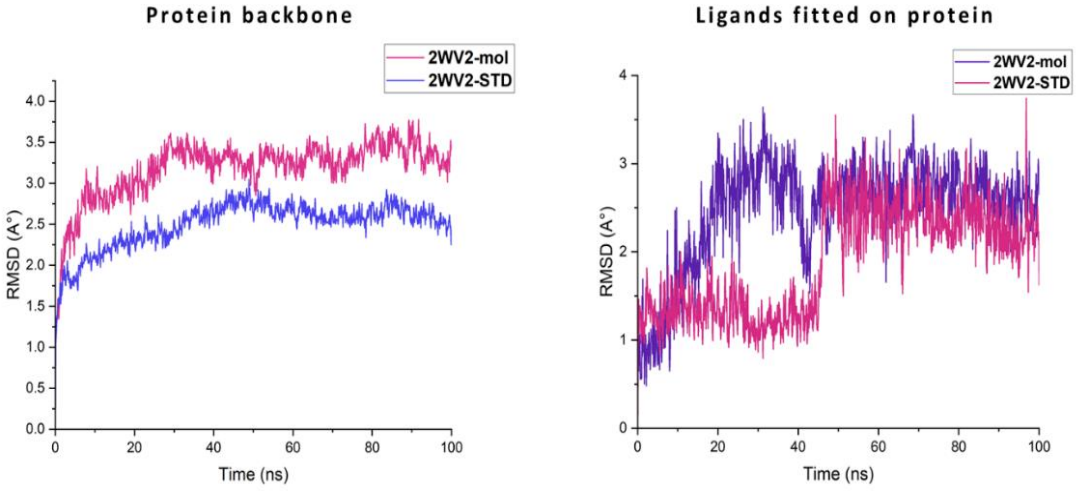

Figure 9. Root Mean Square Deviation plots of studied complex 2WV2-mol in contrast to the standard complex 2WV2-STD with the sterol 14α-demethylase, also known as CYP51 protein.

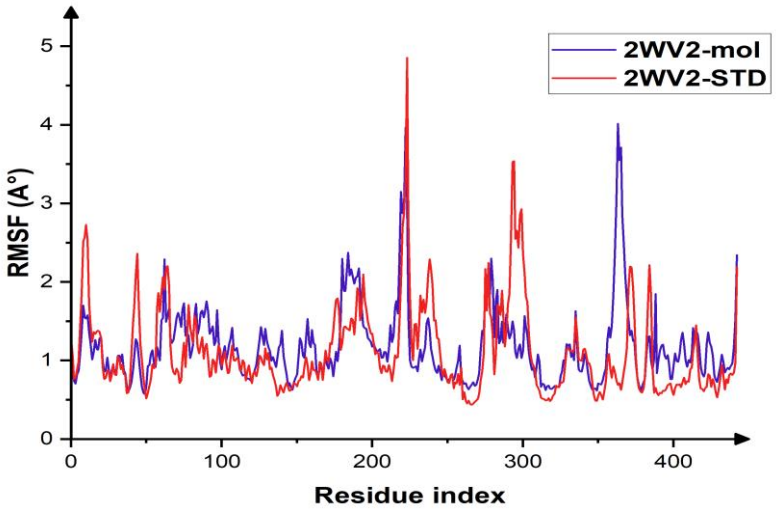

Figure 10. Root Mean Square Fluctuation plots comparing the studied complex 2WV2-Mol to the standard complex 2WV2-STD with the sterol 14α-demethylase, also known as the CYP51 protein.

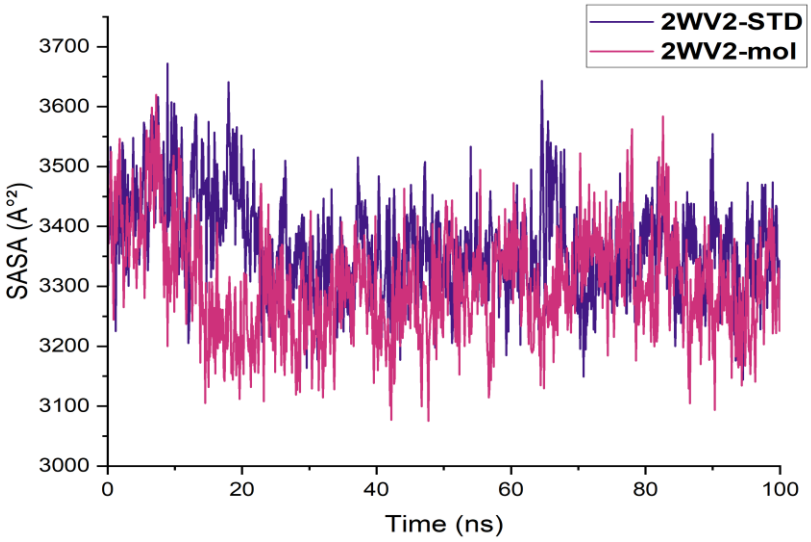

Figure 11. Solvent Accessible Surface Area plots comparing the studied complex 2WV2-Mol to the standard complex 2WV2-STD with the sterol 14α-demethylase, also known as the CYP51 protein.

3.13. Root Mean Square Fluctuatons analysis (RMSF)

Analysing atomic fluctuations through Root Mean Square Fluctuation (RMSF) in Molecular Dynamics (MD) simulations is pivotal for comprehending biomolecular dynamics. A higher RMSF value signifies increased flexibility within the biomolecule's region, while a lower RMSF value indicates rigidity. The RMSF profiles were derived from the fluctuations of alpha carbon atoms in amino acid residues, visually depicted in Fig. 10. These residue-specific fluctuations were meticulously examined for the two complexes mol-2WV2 and STD-2WV2. RMSF average of recorded values was 1.18A° and 1.21A° for mol-2WV2 and STD-2WV2 complexes respectively, hinting at the stabilizing effect of studied compound on the protein residues.

3.14. Solvent accessible surface area and radius of gyration analysis

In our investigation, Solvent Accessible Surface Area (SASA) serves to quantify the portion of the protein that interacts with surrounding solvents within the simulation box. The SASA plot (Fig. 11) illustrates variations that cluster around a relatively stable mean value. Across the complexes 2WV2-Mol and 2WV2-STD, SASA averages were recorded as 3366.52 $Å^2$ and 3304.65 $Å^2$ respectively. Despite these fluctuations, there is no significant deviation from the mean SASA value across the studied compound complex simulations in contrast to the standard ligand complex, indicating a stable interaction between the protein and its surrounding solvent molecules.

Additionally, a radius of gyration (Rg) analysis was conducted to assess the structural attributes of the protein within the investigated system, in comparison to the co-ligand complex (Fig. 12). Generally, Rg changes were consistent across the studied system named 2WV2-mol, indicating stable structural characteristics. The recorded average Rg values for the protein structures were 22.1 Å and 22.3 Å for 2WV2-mol and 2WV2-STD, respectively. These minor discrepancies imply that the protein structures retained a similar compactness in both scenarios.

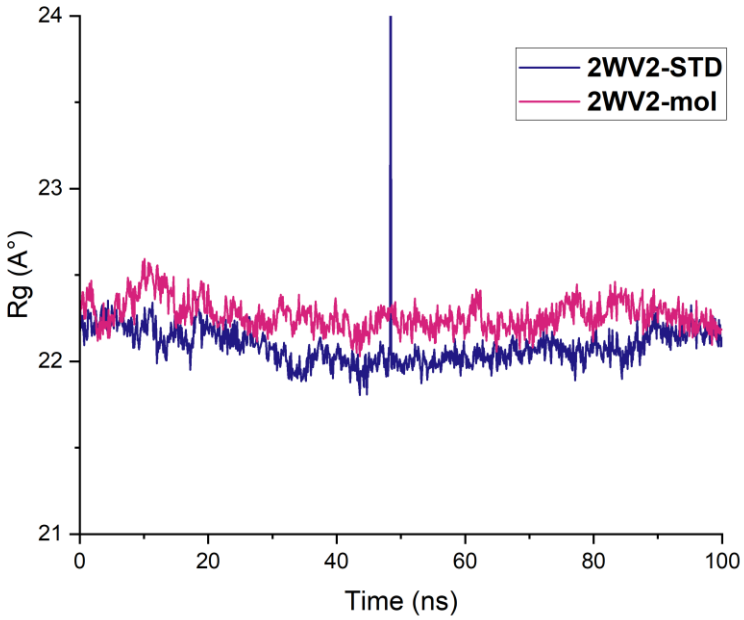

Fig. 12 Radius of gyration plots comparing the studied complex 2WV2-Mol to the standard complex 2WV2-STD with the sterol 14α-demethylase, also known as the CYP51 protein

Table 6 Percentage of Protein Secondary Structure Elements during 100ns MD Simulation across the studied system 2WV2-mol and co-ligand System 2WV2-STD.

Complex	Alpha-Helices	Beta-Strands	SSE%	Loops %
2WY2-mol	32.27	8.16	40.43	58.57
2WY2-STD	36.59	7.91	44.50	55.50

3.15. Protein Secondary Structure analysis

The protein's secondary structure elements, specifically alpha helices and beta strands, are vital in assessing its stability during the 100ns molecular dynamics simulation. A high percentage of secondary structure indicates that the residues are more rigid, whereas the presence of unstructured loop regions suggests flexibility and instability in the protein structure. Fig.13, illustrates the distribution of secondary structure elements by residue index throughout the protein structure. In the case of the molecule of interest the total SSE% of the protein is 40.43 while it is 44.50. These outcomes suggest that the residues of the sterol 14α-

demethylase, also known as the CYP51 protein maintain a stable, rigid structure predominantly in both systems which hint at the stability of formation of the complex with the protein of the studied ligand.

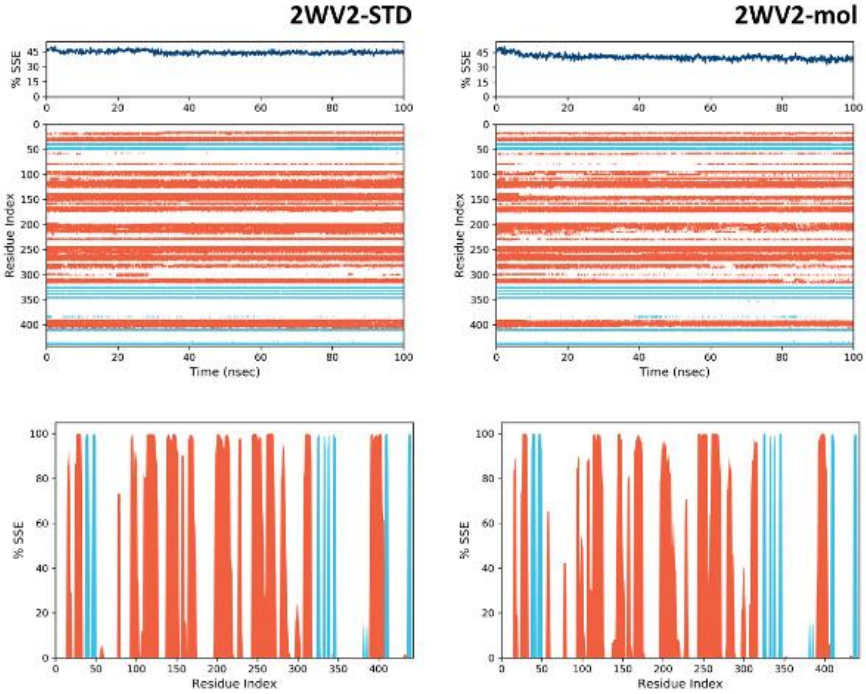

Figure 13. Monitoring Protein Secondary Structure Elements across 100ns MD Simulation: Comparison of systems 2WV2-mol and co-ligand system 2WV2-STD; Alpha-helices highlighted in orange, Beta-strands in blue, and Loops in white.

3.16. Principle Component Analysis and Free-energy Lanscape plots

Principal Component Analysis (PCA) is a statistical method used to simplify protein dynamics data by reducing its dimensionality. This technique highlights the most important motions by sorting them from the largest to the smallest spatial scales. PCA achieves this by performing a linear transformation on a covariance or correlation matrix, which is created from the atomic coordinates that depict the protein's available degrees of freedom (DOF). These coordinates usually comprise Cartesian coordinates that describe atomic movements within trajectory conformations [62].

The PCA data calculated for 2WV2-mol and 2WV2-STD was utilized to create the free energy landscape (FEL) profiles of the systems (Fig. 14). The FEL derived from the PCA data reveals several energy transitions and metastable states, with a few notably large energy wells identified for both systems. However, longer simulations are needed to fully explore the global minima and stable conformations of the structures. The presence of an intense blue area in the last 200 frames of the 2WV2-mol, compared to 2WV2-STD, within the FEL plots indicates that the ligand plays a role in lowering the system's energy relative to the co-ligand system. This underscores the ligand's stabilizing effect over an extended simulation period (Fig. 15).

3.17. MMGBSA calculations

The Prime MMGBSA [63,64] method was employed to assess the relative binding-free energy (ΔG bind) of ligand molecule, along with its individual energy contribution, throughout the 100ns MD simulation. In each step, 100 frames were captured, and the findings are detailed in Table 7 and depicted in Fig. 16. Prime MM-GBSA calculates the energy of optimized free receptors, free ligands, and their complexes. Among the two compounds evaluated, the compound of interest

Mol within the complex 2WV2-mol demonstrated the most favorable binding energy of -63.19 kcal/mol, surpassing the co-ligand present in 2WV2-STD, which exhibited a binding energy of -10.09 kcal/mol.

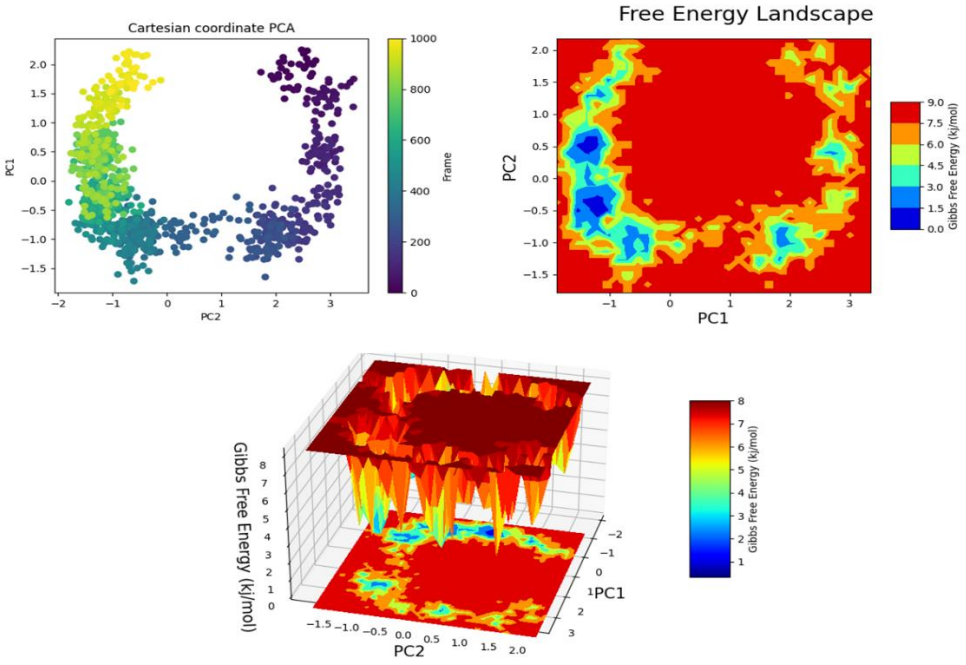

Figure 14. PCA and FEL plots of the protein Cα atoms dynamics evolution 2WV2-STD complex.

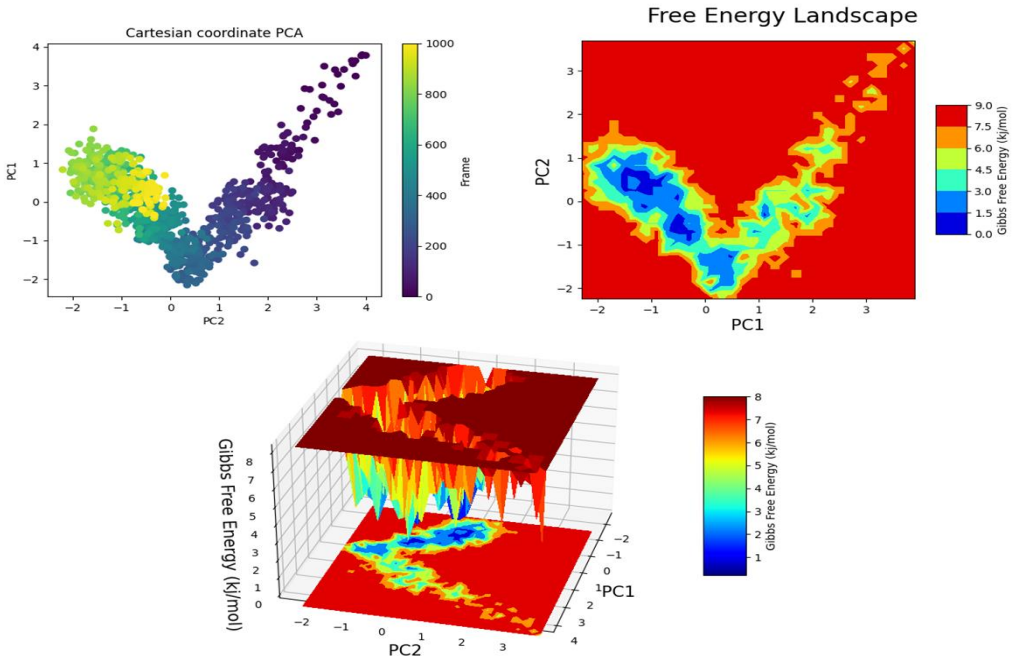

Figure 15. PCA and FEL plots of the protein Cα atoms dynamics evolution 2WV2-mol complex.

Table 7. Summarized Protein-Ligand interactions between the studied molecule and the co-ligand STD with the sterol 14α-demethylase, also known as the CYP51 protein

Complex	Free Energy binding	Electrostatic energy	Van Der Waal	Covalent binding	Hydrogen binding
STD	**-10.09**	**-5.51**	**-39.96**	**1.79**	**-0.085**
Mol	**-63.19**	**-11.95**	**-50.46**	**3.91**	**-0.89**

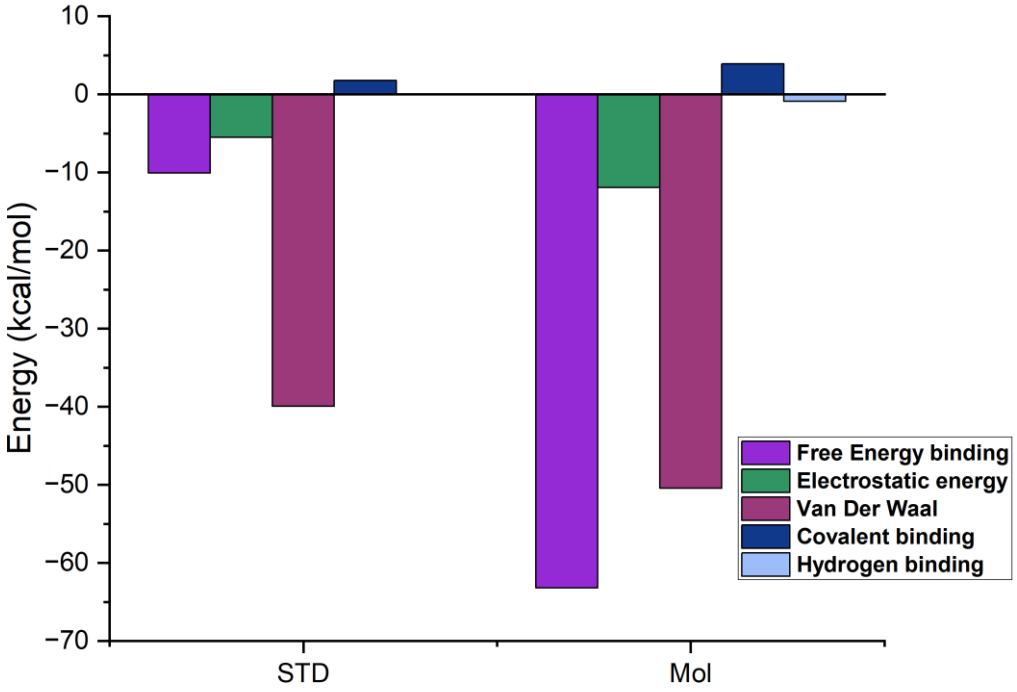

Figure 16 Comparative Analysis of Energy Levels: Binding Energy, Electrostatic Energy, Covalent Binding Energy, Hydrogen Bonding, and Van Der Waals Interactions for the tested complex 2WV2-mol the co-ligand complex 2WV2-STD.

4. Conclusions

Theoretical methods accurately reproduced X-ray geometrical coordinates and quantum chemical parameters for (E)-1-[2-(3,4-Dimethylphenyl)diazen-2-ium-1-yl]naphthalen-2-olate compound (EDNO). Hirshfeld surfaces were employed to confirm and measure the occurrence of intermolecular interactions inside the crystal stack. The molecular docking simulation illustrated the manner in which the (EDNO) molecule interacts with specific residues (amino acids) that are crucial for its inhibitory impact. The connection facilitates the movement of the compound into active protein sites with a binding energy of -10.2 kcal/mol. Our investigation into molecular docking reveals that establishing hydrogen bonds with key amino acids (SER296) in the target protein is crucial for stabilizing ligands inside the active site of the 2WV2 Protein and enhancing their inhibitory effectiveness. A molecular dynamics simulation took place on the docked molecule, which demonstrated significant hydrogen bonding with crucial amino acids of the target protein throughout the simulation. The thermodynamic stability of the molecule was assessed through running the MD simulation for 100 ns. The molecule's thermodynamic stability was evaluated by conducting a 100 ns molecular dynamics (MD) simulation. Consequently, in a biological context, they will probably attach to the target protein and

remain stable. The study's findings clearly suggest that the mentioned compound shows promise as an inhibitor of Corticosteroid side-chain-isomerase

References

[1] S. Benkhaya, S. M'rabet, A. El Harfi, Classifications, properties, recent synthesis and applications of azo dyes, Heliyon 6 (2020) e03271.

[2] C. Luo, O. Borodin, X. Ji, S. Hou, K.J. Gaskell, X. Fan, J. Chen, T. Deng, R. Wang, J. Jiang, C. Wang, Azo compounds as a family of organic electrode materials for alkali-ion batteries, Proc. Natl. Acad. Sci. U.S.A. 115 (2018) 2004–2009.

[3] R. Petruskevicius, D. Urbonas, M. Gabalis, A. Balcytis, G. Seniutinas, R. Tomasiunas, V. Getautis, Optical poling of azo-compounds for applications in nanophotonics, in: 2013 15th International Conference on Transparent Optical Networks (ICTON), IEEE, Cartagena, Spain, 2013: pp. 1–4.

[4] E. Węglarz-Tomczak, Ł. Górecki, Azo dyes–biological activity and synthetic Strategy, Chemik Science-Technique-Market 66 (2012) 1298–1307.

[5] H. Inac, M. Ashfaq, N. Dege, M. Feizi-Dehnayebi, K.S. Munawar, N.K. Yağcı, E. POYRAZ Çınar, M.N. Tahir, Synthesis, spectroscopic characterizations, single crystal XRD, supramolecular assembly inspection via hirshfeld surface analysis, and DFT study of a hydroxy functionalized schiff base Cu(II) complex, Journal of Molecular Structure 1295 (2024) 136751.

[6] I. Sayer, N. Dege, H. Ghalla, A. Moliterni, H. Naïli, Crystal structure, DFT studies and thermal characterization of new luminescent stannate (IV) based inorganic-organic hybrid compound, Journal of Molecular Structure 1224 (2021) 129266.

[7] S. Şahin, N. Dege, Synthesis, characterization, X-ray, HOMO-LUMO, MEP, FT-IR, NLO, Hirshfeld surface, ADMET, boiled-egg model properties and molecular docking studies with human cyclophilin D (CypD) of a Schiff base compound: (E)-1-(5-nitro-2-(piperidin-1-yl)phenyl)-N-(3-nitrophenyl)methanimine, Polyhedron 205 (2021) 115320.

[8] G. Demirtaş, N. Dege, H. İçbudak, Ö. Yurdakul, O. Büyükgüngör, Experimental and DFT Studies on Poly[di-μ3-acesulfamato-O,O:O′;O′:O,O-di-μ-acesulfamato-O,O; N-di-μ-aqua-dicalcium(II)] Complex, J Inorg Organomet Polym 22 (2012) 671–679.

[9] E. Banaszak-Leonard, A. Fayeulle, A. Franche, S. Sagadevan, M. Billamboz, Antimicrobial azo molecules: a review, J IRAN CHEM SOC 18 (2021) 2829–2851.

[10] M. Di Martino, L. Sessa, M. Di Matteo, B. Panunzi, S. Piotto, S. Concilio, Azobenzene as Antimicrobial Molecules, Molecules 27 (2022) 5643.

[11] N.A. Razali, Z. Jamain, Liquid Crystals Investigation Behavior on Azo-Based Compounds: A Review, Polymers 13 (2021) 3462.

[12] X. Wang, Introduction, in: Azo Polymers, Springer Berlin Heidelberg, Berlin, Heidelberg, 2017: pp. 1–17.

[13] S. Hamamci Alisir, N. Dege, R. Tapramaz, Synthesis, crystal structures and characterizations of three new copper(II) complexes including anti-inflammatory diclofenac, Acta Cryst C 75 (2019) 388–397.

[14] N. Dege, H. İçbudak, E. Adıyaman, Bis(acesulfamato-κ2O4,N)bis(3-methyl-pyridine)copper(II), Acta Cryst C 62 (2006) m401–m403.

[15] R. Pino-Rios, E. Pino, G. Cárdenas-Jirón, Deciphering the origin of the first steps in the degradation of azo dyes: a computational study, Environ Sci Pollut Res 31 (2023) 657–667.

[16] Ö. Tamer, N. Dege, D. Avcı, Y. Atalay, İ. Özer İlhan, M. Çadır, Synthesis, structural and spectroscopic evaluations and nonlinear optical properties of 3,5-bis(4-methoxyphenyl)-4,5-dihydro-1H-pyrazole-1-carbothioic O-acid, Spectrochimica Acta Part A: Molecular and Biomolecular Spectroscopy 137 (2015) 1387–1396.

[17] Ö. Tamer, N. Dege, G. Demirtaş, D. Avcı, Y. Atalay, M. Macit, A.A. Ağar, An experimental and theoretical study on the novel (Z)-1-((naphthalen-2-ylamino)methylene)naphthalen-2(1H)-one crystal, Spectrochimica Acta Part A: Molecular and Biomolecular Spectroscopy 117 (2014) 13–23.

[18] Dotse Selali Chormey, B.T. Zaman, E. Maltepe, Ç. Büyükpınar, A.E. Bulgurcuoğlu,

F. Turak, F.A. Erulaş, S. Bakırdere, Simultaneous Determination of Harmful Aromatic Amine Products of Azo Dyes by Gas Chromatography–Mass Spectrometry, J Anal Chem 75 (2020) 1330–1334.

[19] N. Dege, M.A. Raza, O.E. Doğan, T. Ağar, M.W. Mumtaz, Theoretical and experimental approaches of new Schiff bases: efficient synthesis, X-ray structures, DFT, molecular modeling and ADMET studies, J IRAN CHEM SOC 18 (2021) 2345–2368.

[20] F.E. Kalai, E.B. Çınar, C.-H. Lai, S. Daoui, T. Chelfi, M. Allali, N. Dege, K. Karrouchi, N. Benchat, Synthesis, spectroscopy, crystal structure, TGA/DTA study, DFT and molecular docking investigations of (E)-4-(4-methylbenzyl)-6-styrylpyridazin-3(2H)-one, Journal of Molecular Structure 1228 (2021) 129435.

[21] M. J. Frisch, G. W. Trucks, H. B. Schlegel, G. E. Scuseria, M. A. Robb, J. R. Cheeseman, G. Scalmani, V. Barone, G. A. Petersson, H. Nakatsuji, X. Li, M. Caricato, A. V. Marenich, J. Bloino, B. G. Janesko, R. Gomperts, B. Mennucci, H. P. Hratchian, J. V. Ortiz, A. F. Izmaylov, J. L. Sonnenberg, D. Williams-Young, F. Ding, F. Lipparini, F. Egidi, J. Goings, B. Peng, A. Petrone, T. Henderson, D. Ranasinghe, V. G. Zakrzewski, J. Gao, N. Rega, G. Zheng, W. Liang, M. Hada, M. Ehara, K. Toyota, R. Fukuda, J. Hasegawa, M. Ishida, T. Nakajima, Y. Honda, O. Kitao, H. Nakai, T. Vreven, K. Throssell, J. A. Montgomery, Jr., J. E. Peralta, F. Ogliaro, M. J. Bearpark, J. J. Heyd, E. N. Brothers, K. N. Kudin, V. N. Staroverov, T. A. Keith, R. Kobayashi, J. Normand, K. Raghavachari, A. P. Rendell, J. C. Burant, S. S. Iyengar, J. Tomasi, M. Cossi, J. M. Millam, M. Klene, C. Adamo, R. Cammi, J. W. Ochterski, R. L. Martin, K. Morokuma, O. Farkas, J. B. Foresman, and D. J. Fox, Gaussian, Inc., Wallingford CT, (2016) (n.d.).

[22] R.D.T.K.J. Millam, Shawnee Mission KS. GaussView, Semichem Inc. (2009). (n.d.).

[23] P.R. Spackman, M.J. Turner, J.J. McKinnon, S.K. Wolff, D.J. Grimwood, D. Jayatilaka, M.A. Spackman, CrystalExplorer: a program for Hirshfeld surface analysis, visualization and quantitative analysis of molecular crystals, J Appl Cryst 54 (2021) 1006–1011.

[24] T. Lu, F. Chen, Multiwfn: A multifunctional wavefunction analyzer, J Comput Chem 33 (2012) 580–592.

[25] W. Humphrey, A. Dalke, K. Schulten, VMD: Visual molecular dynamics, Journal of Molecular Graphics 14 (1996) 33–38.

[26] O. Trott, A.J. Olson, AutoDock Vina: Improving the speed and accuracy of docking with a new scoring function, efficient optimization, and multithreading, J Comput Chem 31 (2010) 455–461.

[27] G.M. Morris, R. Huey, W. Lindstrom, M.F. Sanner, R.K. Belew, D.S. Goodsell, A.J. Olson, AutoDock4 and AutoDockTools4: Automated docking with selective receptor flexibility, Journal of Computational Chemistry 30 (2009) 2785–2791.

[28] BIOVIA, Life Sciences and Material Sciences | BIOVIA – Dassault Systèmes. Https://Www.3ds.Com/Products-Services/Biovia/(Accessed June 6, 2022) (n.d.).

[29] B. Dziuk, B. Ośmiałowski, A. Skotnicka, K. Ejsmont, B. Zarychta, 2-[4-(Dimethylamino)phenyl]-3,3-difluoro-3 *H* -naphtho[1,2- *e*][1,3,2]oxazaborinin-2-ium-3-uide, IUCrData 2 (2017) x171141.

[30] M.J. Márquez, M.B. Márquez, P.G. Cataldo, S.A. Brandán, A Comparative Study on the Structural and Vibrational Properties of Two Potential Antimicrobial and Anticancer Cyanopyridine Derivatives, OJSTA 04 (2015) 1–19.

[31] A. Dhandapani, S. Veeramanikandan, R.S. Kumar, A.I. Almansour, N. Arumugam, S. Subashchandrabose, J. Suresh, R. Arulraj, D. Gajalakshmi, Synthesis, in vitro and in silico antitumor evaluation of 3-(2,6-dichlorophenyl)-1,5-diphenylpentane-1,5-dione: Structure, spectroscopic, RDG, Hirshfeld and DFT based analyses, Journal of Molecular Structure 1251 (2022) 132002.

[32] P. Agarwal, S. Bee, A. Gupta, P. Tandon, V.K. Rastogi, S. Mishra, P. Rawat, Quantum chemical study on influence of intermolecular hydrogen bonding on the geometry, the atomic charges and the vibrational dynamics of 2,6-dichlorobenzonitrile, Spectrochimica Acta Part A: Molecular and Biomolecular Spectroscopy 121 (2014) 464–482.

[33] E.R. Johnson, S. Keinan, P. Mori-Sánchez, J. Contreras-García, A.J. Cohen, W. Yang, Revealing Noncovalent Interactions, J. Am. Chem. Soc. 132 (2010) 6498–6506.

[34] M.A. Spackman, P.G. Byrom, A novel definition of a molecule in a crystal, Chemical Physics Letters 267 (1997) 215–220.

[35] M. Ashfaq, K.S. Munawar, G. Bogdanov, A. Ali, M.N. Tahir, G. Ahmed, A. Ramalingam, M.M. Alam, M. Imran, S. Sambandam, B. Munir, Single crystal inspection, Hirshfeld surface investigation and DFT study of a novel derivative of 4-fluoroaniline: 4-((4-fluorophenyl)amino)-4-oxobutanoic acid (BFAOB), J IRAN CHEM SOC 19 (2022) 1953–1961.

[36] P.R. Spackman, M.J. Turner, J.J. McKinnon, S.K. Wolff, D.J. Grimwood, D. Jayatilaka, M.A. Spackman, CrystalExplorer: a program for Hirshfeld surface analysis, visualization and quantitative analysis of molecular crystals, J Appl Cryst 54 (2021) 1006–1011.

[37] M.A. Spackman, J.J. McKinnon, Fingerprinting intermolecular interactions in molecular crystals, CrystEngComm 4 (2002) 378–392.

[38] S.A. Kaas, F.T. Baara, Y. Megrouss, S. Yahiaoui, A. Djafri, F.Z. Boudjenane, A. Chouaih, A. Djafri, A. Hatzidimitriou, Synthesis, crystal structure, Hirshfeld surface analysis, computational investigations and molecular docking studies of (Z)-3-N-(methyl)-2-N'-(4-methoxyphenylimino) thiazolidin-4-one dihydrate, Journal of Molecular Structure 1308 (2024) 137964.

[39] S. Yahiaoui, Y. Megrouss, N. Boukabcha, N. El Houda Belkafouf, N. Khelloul, R. Rahmani, N. Boubegra, A. Chouaih, Structural characterization, molecular docking assessment, drug-likeness study and DFT investigation of 2-(2-{1,2-dibromo-2-[3-(4-chloro-phenyl)-[1,2,4]oxadiazol-5-yl]-2-fluoro-ethyl1}-phenyl)-methyl 3-methoxy-acrylic ester, Journal of the Indian Chemical Society 99 (2022) 100745.

[40] S. Akash, F.I. Aovi, Md.A.K. Azad, A. Kumer, U. Chakma, Md.R. Islam, N. Mukerjee, Md.M. Rahman, I. Bayıl, S. Rashid, R. Sharma, A drug design strategy based on molecular docking and molecular dynamics simulations applied to development of inhibitor against triple-negative breast cancer by Scutellarein derivatives, PLoS ONE 18 (2023) e0283271.

[41] A.A. Basha, A. Kubaib, M. Azam, Exploring the antiviral potency of γ-FP and PA compounds: Electronic characterization, non-covalent interaction analysis and docking profiling with emphasis on QTAIM aspects, Computational and Theoretical Chemistry 1231 (2024) 114412.

[42] M.C. Walker, A. Marandici, K. Martin, C. Monder, Genetic Control of Corticosteroid Side-Chain Isomerase Activity in the Mouse*, Endocrinology 112 (1983) 924–930.

[43] C. Monder, A. Marandici, Corticosteroid side-chain isomerase in the circulatory system, Steroids 56 (1991) 12–16.

[44] L.A.R. Sallam, A.-M. El-Refai, H.A. El-Minofi, Physiological and biochemical improvement of the enzyme side-chain degradation of cholesterol by Fusarium solani, Process Biochemistry 40 (2005) 203–206.

[45] M. Mutsuga, Y. Asaoka, N. Imura, T. Miyoshi, Y. Togashi, Aminoglutethimide-induced lysosomal changes in adrenal gland in mice, Experimental and Toxicologic Pathology 69 (2017) 424–429.

[46] H. Ferjani, R. Bechaieb, N. Dege, W.A. El-Fattah, N.Y. Elamin, W. Frigui, Stabilization of supramolecular network of fluconazole drug polyiodide: Synthesis, computational and spectroscopic studies, Journal of Molecular Structure 1263 (2022) 133192.

[47] X. Qi, Y. Zhao, Z. Qi, S. Hou, J. Chen, Machine Learning Empowering Drug Discovery: Applications, Opportunities and Challenges, Molecules 29 (2024) 903.

[48] M. Mandal, S. Mandal, MM/GB(PB)SA integrated with molecular docking and ADMET approach to inhibit the fat-mass-and-obesity-associated protein using bioactive compounds derived from food plants used in traditional Chinese medicine, Pharmacological Research - Modern Chinese Medicine 11 (2024) 100435.

[49] J. Dulsat, B. López-Nieto, R. Estrada-Tejedor, J.I. Borrell, Evaluation of Free Online ADMET Tools for Academic or Small Biotech Environments, Molecules 28 (2023) 776.

[50] V. Manakkadan, J. Haribabu, V.N.V. Palakkeezhillam, P. Rasin, M. Mandal, V.S. Kumar, N. Bhuvanesh, R. Udayabhaskar, A. Sreekanth, Synthesis and characterization of N-substituted thiosemicarbazones: DNA/BSA binding, molecular docking, anticancer activity, ADME study and computational investigations, Journal of Molecular Structure 1285 (2023) 135494.

[51] Z. Fralish, A. Chen, P. Skaluba, D. Reker, DeepDelta: predicting ADMET improvements of molecular derivatives with deep learning, J Cheminform 15 (2023) 101.

[52] C.M. Chagas, S. Moss, L. Alisaraie, Drug metabolites and their effects on the development of adverse reactions: Revisiting Lipinski's Rule of Five, International Journal of Pharmaceutics 549 (2018) 133–149.

[53] R.N. Sahoo, S. Pattanaik, G. Pattnaik, S. Mallick, R. Mohapatra, Review on the use of Molecular Docking as the First Line Tool in Drug Discovery and Development, IJPS 84 (2022).

[54] P.C. Agu, C.A. Afiukwa, O.U. Orji, E.M. Ezeh, I.H. Ofoke, C.O. Ogbu, E.I. Ugwuja, P.M. Aja, Molecular docking as a tool for the discovery of molecular targets of nutraceuticals in diseases management, Sci Rep 13 (2023) 13398.

[55] H.M. Berman, The Protein Data Bank, Nucleic Acids Research 28 (2000) 235–242.

[56] C.-K. Chen, S.S.F. Leung, C. Guilbert, M.P. Jacobson, J.H. McKerrow, L.M. Podust, Structural Characterization of CYP51 from Trypanosoma cruzi and Trypanosoma brucei Bound to the Antifungal Drugs Posaconazole and Fluconazole, PLoS Negl Trop Dis 4 (2010) e651.

[57] I. Sama-ae, N.C. Pattaranggoon, A. Tedasen, In silico prediction of Antifungal compounds from Natural sources towards Lanosterol 14-alpha demethylase (CYP51) using Molecular docking and Molecular dynamic simulation, Journal of Molecular Graphics and Modelling 121 (2023) 108435.

[58] R. Zhang, Y. Wang, A. Wu, J. Wang, J. Zhang, Strategies of targeting CYP51 for IFIs therapy: Emerging prospects, opportunities and challenges, European Journal of Medicinal Chemistry 259 (2023) 115658.

[59] N. Khelfa, S. Belaidi, O. Abchir, I. Yamari, S. Chtita, A. Samadi, M.M. Al-Mogren, M. Hochlaf, Combined 3D-QSAR, molecular docking, ADMET, and drug-likeness scoring of novel diaminodihydrotriazines as potential antimalarial agents, Scientific African 24 (2024) e02202.

[60] K.J. Bowers, F.D. Sacerdoti, J.K. Salmon, Y. Shan, D.E. Shaw, E. Chow, H. Xu, R.O. Dror, M.P. Eastwood, B.A. Gregersen, J.L. Klepeis, I. Kolossvary, M.A. Moraes, Molecular dynamics---Scalable algorithms for molecular dynamics simulations on commodity clusters, in: Proceedings of the 2006 ACM/IEEE Conference on Supercomputing - SC '06, ACM Press, Tampa, Florida, 2006: p. 84.

[61] E. Harder, W. Damm, J. Maple, C. Wu, M. Reboul, J.Y. Xiang, L. Wang, D. Lupyan, M.K. Dahlgren, J.L. Knight, J.W. Kaus, D.S. Cerutti, G. Krilov, W.L. Jorgensen, R. Abel, R.A. Friesner, OPLS3: A Force Field Providing Broad Coverage of Drug-like Small Molecules and Proteins, J. Chem. Theory Comput. 12 (2016) 281–296.

[62] C.C. David, D.J. Jacobs, Principal Component Analysis: A Method for Determining the Essential Dynamics of Proteins, in: D.R. Livesay (Ed.), Protein Dynamics, Humana Press, Totowa, NJ, 2014: pp. 193–226.

[63] M.P. Jacobson, D.L. Pincus, C.S. Rapp, T.J.F. Day, B. Honig, D.E. Shaw, R.A. Friesner, A hierarchical approach to all-atom protein loop prediction, Proteins 55 (2004) 351–367.

[64] M.P. Jacobson, R.A. Friesner, Z. Xiang, B. Honig, On the Role of the Crystal Environment in Determining Protein Side-chain Conformations, Journal of Molecular Biology 320 (2002) 597–608.